Kinematic Observers For Articulated Rovers

J. (Bob) Balaram
Jet Propulsion Laboratory, California Institute of Technology
4800 Oak Grove Drive, Pasadena, California 91109, USA

Abstract

A state estimator design is presented for a Mars rover prototype. Odometry estimates are obtained by utilizing the full kinematics of the vehicle including the nonlinear internal kinematics of the rover rocker-bogey mechanism as well as the contact kinematics between the wheels and the ground. Additional sensing using gyroscopes, acclerometers and visual sensors allows for robust rover motion state estimation. Simulation as well as experimental results are presented to illustrate the estimator operation.

1 Introduction

Future space missions to Mars include science rovers in '03 and '05 and other rovers in support of Mars Outpost activities in the following decades. Unlike the Sojourner rover on the recent Pathfinder mission, a long-range rover will traverse many kilometers away from a lander. Such a rover will not be able to rely on navigation methods based upon images obtained by the lander stereoscopic cameras. While some position estimation will be possible using intermittent interaction with orbital assets, and lander/rover deployed GPS-type pseudo-lites may be available at some sites, a robust state estimation framework relying on onboard sensors is important for mission success.

In this paper we focus on non-visual methods of state estimation. Such methods are important in their own right since they serve as backup to vision-based methods in regions of low visual content. They also allow visual feature tracking and range map matching methods to be more robust to failure, reduce search/computation costs, and minimize the number of imaging related mast deployment operations.

The paper describes a method to improve the precision of the odometry estimate by using the full kinematics of the rocker/bogey mechanisms of the rover as it traverses undulating/bumpy terrain. This is considerably more complex than a kinematically simpler vehicle operating on a flat indoor environment. The Kalman filtering framework adopted also provides a natural Bayesian means of combining any visually based motion estimates into the full state estimate.

1.1 Rocky-7 Research Platform

Many of the future Mars rovers are planned to have an articulated rocker-bogey suspensions mechanism, 6-wheel driving, and 2-6 wheel steering. A research prototype vehicle with some of these characteristics is the Rocky-7 rover research platform [19] shown in Figure 1. The mobility system consists of 6 drive wheels,

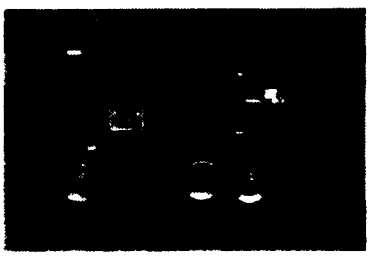

Figure 1: Rocky-7 Side View

2 steering wheels, rockers hinged to the sides of the main body connected by a differential, and bogey assemblies at each end of the rocker. Sensors include a solar-panel mounted sun-sensor, a vibratory heading gyro, and a 3-axis accelerometer. Internal angles of the rover mechanism are read by potentiometers. Wheel drive and steering angles are read by optical encoders. The rover is equipped with 7 CCD cameras, 2 at each end for the hazard avoidance system and 3 on the mast (2 for stereo panaromas, and 1 for close-up viewing).

1.2 Previous Work

We briefly describe some representative related work in the area of mobile robot state estimation. Since Global Positioning System (GPS) based methods are

not generally applicable to a vehicle on Mars, we have excluded them from our discussion.

Beacon-based localization has been considered by Leonard [9] in which an Extended Kalman Filter (EKF) is employed to match environment observations to a map. Matthies [12] used a Kalman Filtering approach to track stereo vision features and obtain vehicle motion. Baumgartner and Skaar [2] estimate a vehicle's position and orientation based on visual cues in discrete locations within a structured environment. Olson [15] utilizes range map matching to periodically localize a mobile vehicle.

Borenstein and Feng [3] develop a technique where gyro data is only used when the gyro and odometry estimates differ. Barshan and Durrant-Whyte [1] use inertial sensors in an EKF to estimate position. Vaganay and Aldon [18] utilize accelerometers and gyros for vehicle attitude estimation. Fuke and Krotkov [6] utilize gyros and accelerometers together with odometry to estimate vehicle attitude. The combination of gyro and sun-sensor data for vehicle attitude estimation is addressed by Roumeliotis and Bekey [16].

Kinematic techniques include an effort by Kim, et.al [8] to extend a dead-reckoning formula for a two-wheeled robot on a known curved surface. Slip modeling for a vehicle operating in the plane is considered by Madhavan, et. al [11] where a random walk model for a slip angle parameter is used for estimating the motion of a truck with planar articulation elements.

2 Rover Model

Here we discuss the model used for rover state estimation. This consists of a state-space model to propagate rover position and attitude, a kinematic contact model to describe wheel interactions with the ground, and measurement models for the sensors.

2.1 Coordinate Frames and Variables

Coordinate frames and variables are as defined in Figure 2. The unconstrained rover's degrees-of-freedom (dof's) are seen to be three translational, three rotational, three internal $(\gamma_0, \gamma_1, \gamma_2)$, two steering (λ_1, λ_2), and six drive $(\psi_1, \ldots, \psi_6)$. Contact at each wheel constrains these dof's to two translational dof's (x,y) and one angular dof (heading) when the rover is in full contact with the ground.

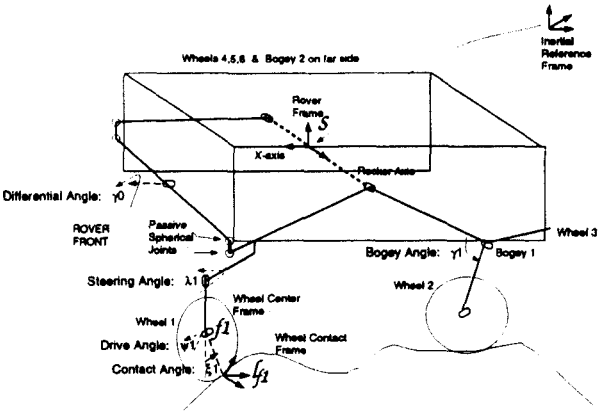

Figure 2: Rocky-7 Kinematics

2.2 Process Model

The process model may be chosen so that the sensor data is used as an input to drive the process equation. Alternatively, dynamic models for the process can be introduced, and the sensor information can be captured by a separate measurement equation.

Treating the sensor data as inputs obviates the need to introduce higher order states into the process model. It avoids the difficulty of modeling detailed process dynamics and allows the filter to be responsive to high-frequency motions without excessive low-pass filtering. The so-called *complementary* property of such filters is further discussed in Appendix A.

In cases where there is insufficient sensor data to drive all the terms in the process equation, we adopt a hybrid approach. The available data is used to drive part of the state equation, and a process model with simple dynamics is used for the rest. Such an approach is necessitated in the case of the attitude evolution model for those rovers that implement only a heading gyro (such as Rocky-7).

2.2.1 Attitude State Model

Here we adopt a hybrid form combining both a heading gyro measurement and a simple noise driven process dynamics.

$$\begin{bmatrix} \dot{q} \\ \dot{\omega}_p \end{bmatrix} = \begin{bmatrix} \frac{1}{2}\Omega(\omega)q \\ 0 \end{bmatrix} + \begin{bmatrix} 0 \\ n_\omega \end{bmatrix} \quad (1)$$

All angular variables are resolved in body coordinate with $q \in R^4$ being the attitude unit quaternion. The total body angular velocity ω is the sum of three terms

$\omega = \omega_m + \omega_p + b$, with $\omega_m, \omega_p, b \in R^3$. The ω_m is the measured gyro value and will be non-zero only for the z-axis component of the body angular velocity. The ω_p then represents a perturbation angular velocity which is driven by an angular acceleration noise n_ω. As we are measuring the z-axis angular velocity, the corresponding noise term is taken to be small. The b represents the gyro bias. The terms in quaternion evolution equation are:

$$\Omega(\omega) \triangleq \begin{bmatrix} -\omega^\times & \omega \\ -\omega^T & 0 \end{bmatrix}; \quad \omega^\times \triangleq \begin{bmatrix} 0 & -\omega_3 & \omega_2 \\ \omega_3 & 0 & -\omega_1 \\ -\omega_2 & \omega_1 & 0 \end{bmatrix} \tag{2}$$

Small Angle Evolution

We define an intermediate local model to which the standard continuous-discrete Extended Kalman Filter (EKF) equations can be applied [7]. Because the normalization constraint $q^T q = 1$ is not explicitly enforced in the estimator design, the quaternion q acts as an over-parameterized representation of the 3-axis attitude. In order to avoid the redundant state, a local vector angular variable $\theta \in \mathcal{R}^3$ is defined by a local linearization at the beginning of each propagation step. After the completion of the corresponding update step, the local angular variable is absorbed into the quaternion from the previous linearization. The process is continued with subsequent linearizations. The corresponding covariance terms are maintained in terms of the local angular variable, which characterizes a ball of uncertainty about the attitude estimate. The linearized equation for θ becomes [17]:

$$\dot{\theta} = \omega - \frac{1}{2}\omega^\times \theta \tag{3}$$

Note that this parameterization is linear in θ but preserves the nonlinear dependence of ω for this accuracy in θ. This is a locally valid nonlinear system which remains to be *further* linearized in the usual EKF sense.

2.2.2 Translation State Model

Here the data from a 3-axis accelerometer is used to drive the process.

$$\begin{bmatrix} {}^{\mathcal{I}}\dot{x} \\ \dot{v} \end{bmatrix} = \begin{bmatrix} R(q)v \\ a_m + R^T(q)g - (\omega^\times v + \omega^\times \omega^\times L^b + \dot{\omega}^\times L^b) \end{bmatrix} + \begin{bmatrix} 0 \\ n_v \end{bmatrix} \tag{4}$$

The translational position ${}^{\mathcal{I}}x \in R^3$, of the rover frame is resolved in the inertial frame. However, the velocity $v \in R^3$ is resolved in the body frame. The matrix $R(q)$ is the rotation matrix of the rover attitude as a function of q, the attitude quaternion. The accelerometer frame is assumed to be aligned with the rover frame. The term L^b is the vector from the rover frame to the accelerometer frame origin.

2.2.3 Contact State Model

$$\begin{bmatrix} \dot{\xi} \end{bmatrix} = \begin{bmatrix} A_\xi \xi \end{bmatrix} + \begin{bmatrix} n_\xi \end{bmatrix} \tag{5}$$

The contact point vector $\xi = \{\xi_1, \xi_2, \xi_3, \xi_4, \xi_5, \xi_6\}$ is modeled very simply as a set of one parameter contacts about the equator of each wheel, with the nominal contact position $\xi_i = 0$. In reality there is an additional off-equatorial coordinate for the contact point at each wheel, a contact rotation angle, and two parameters that describe the point on the ground [13]. However the one parameter model suffices to capture and couple the rotational and translational velocities. We can also reduce the number of contact state variables to four by noting that for terrain with moderate curvature the contact points on each wheel of a bogey set are almost symmetrical and can be modeled with a single contact state. The dynamics encoded in A_ξ is used to return the contact point eventually to the nominal position. This ensures correct steady-state behavior when travelling on flat surfaces.

2.2.4 Gyro Bias

The gyro bias can be modeled as a random walk and successive measurement of all three attitude components by an absolute sensor would allow this bias to be estimated while the rover is in motion. However, since the Mars rover operations call for the rover to periodically come to a stop (every few meters), bias can be simply estimated by averaging the gyro data during these times when the rover is stopped. Therefore we choose to not incorporate a gyro bias process model into the state estimator.

2.3 Measurement Model

As we have already absorbed the gyro and acceleration measurements into the process model, here we discuss only the other sensor quantities such as the sun-sensor. We also address the nonlinear kinematics by means of slip related constraint that we treat in a manner similar to that of a measurement.

2.3.1 Sun-Sensor Model

The sun-sensor design is a wide-angle lens which projects an image of the sky on a two-dimensional position sensing device [5]. The output currents of this device, specifically the ratio of currents for each dimension, provides the position of the centroid, s_m, of the Sun's image from the edge of the device.

The sun-sensor has optics most easily described by a fish-eye lens model. In the sun-sensor frame, the sun azimuth angle is given by $atan(s_m(2), -s_m(1))$, and elevation by $\pi/2(1 - \sqrt{s_m(1)^2 + s_m(2)^2})$. Equivalently, the output of the sensor can be expressed in terms of of the two independent components of the sun unit vector resolved in the sun-sensor frame:

$$\begin{bmatrix} s_m \end{bmatrix} = (2/\pi)\frac{\arcsin(\sqrt{s_x^2 + s_y^2})}{\sqrt{s_x^2 + s_y^2}} \begin{bmatrix} s_x \\ s_y \end{bmatrix} + \begin{bmatrix} n_s \end{bmatrix} \quad (6)$$

$$\begin{bmatrix} s_x \\ s_y \end{bmatrix} = \begin{bmatrix} 1 & 0 & 0 \\ 0 & 1 & 0 \end{bmatrix} R^T(q) s_v \quad (7)$$

The unit vector s_v represents the sun-vector in inertial coordinates. This vector is rotated into the sun-sensor coordinate system (which is taken to be the rover frame) by the matrix $R(q) \in R^{3\times3}$ corresponding to the quaternion q. The noise term n_s lumps the effects of electronics noise as well as calibration errors.

2.3.2 Kinematic Slip Model

There is no simple analytical formulation of the inverse kinematics map that relates wheel rotations and contact interactions to the vehicle motion. Such a map must necessarily involve the dynamics of the vehicle and is too complicated for implementation in the filter. Instead we choose to embed the easily established forward kinematics within a *constraint* that is treated as a *measurement* in the filter. We shall see that this allows a natural implementation of the full kinematics of the vehicle. It exploits the ability of the Kalman filter to perform the appropriate least-squares averaging of the action of each kinematic chain in the rover.

Each such forward kinematic chain has a component defined by sequence of links joining the rover frame to each wheel contact point, and a component given by the slip between the wheel and the ground. We introduce the notion of a slip measurement or constraint, t_{m_i}, that defines the relative 6-dof motion of the contact frame l_{fi} (see Figure 2) on the wheel with respect to the ground. This slip is a function of the vehicle configuration, the 6-dof vehicle velocity, the wheel-to-ground contact point location, and the joint rates associated with the kinematic chain emanating from the rover frame to the contact point.

$$t_{m_i} = B^T Ad^{-1}_{g_{sl_{f_i}}}(\gamma, \lambda, \xi_i) * \left(\begin{bmatrix} v \\ \omega \end{bmatrix} + J^s_{sf_i}(\gamma, \lambda) \begin{bmatrix} \dot{\gamma} \\ \dot{\lambda} \\ \dot{\psi} \end{bmatrix} \right) + \begin{bmatrix} n_{t_i} \end{bmatrix} \quad (8)$$

The Ad_g^{-1} term is the Adjoint Operator [14] given by:

$$Ad_g^{-1} = \begin{bmatrix} R^T & -R^T p^\times \\ 0 & R^T \end{bmatrix}; \quad p^\times \triangleq \begin{bmatrix} 0 & -p_3 & p_2 \\ p_3 & 0 & -p_1 \\ -p_2 & p_1 & 0 \end{bmatrix} \quad (9)$$

The term $g_{sl_{f_i}}$ represents the transformation from the rover frame to the contact point. The term $J^s_{sf_i}$ represents the Spatial Jacobian [14] to each wheel center and is a function of the kinematics of the rover.

Here the internal angles are represented by γ, the steering angles by λ, the drive angles by ψ, and the contact point by ξ_i. The terms Ad_g^{-1} is a function of γ, λ, and ξ. However, it is not a function of the driving angles ψ because of rotational symmetry of the wheel. The term $J^s_{sf_i}$ is also not a function of the driving angles ψ and is only a function of γ and λ.

A variety of choices are possible for the B matrices. We adopt the B matrix for pure rolling:

$$B = \begin{bmatrix} 1 & 0 & 0 & 0 \\ 0 & 1 & 0 & 0 \\ 0 & 0 & 1 & 0 \\ 0 & 0 & 0 & 0 \\ 0 & 0 & 0 & 0 \\ 0 & 0 & 0 & 1 \end{bmatrix} \quad (10)$$

This slip constraint measurement can be decomposed into a known deterministic component and a component that is only known in a statistical sense. The deterministic component of the slip, indicated by a nonzero nominal value of t_m, is used to capture the effects of a known steering action. For example, a known rotational slip about the vertical is always present at each wheel to accommodate the yaw motion of the vehicle during a turn. Also, some transverse slip is introduced due to the nature of the non-steered bogey wheels on a rover like Rocky-7. In this case, the bogey wheels have their rotation axis on two parallel lines longitudinally (x) offset from each other. As a consequence there is always some transverse slip even during an Ackerman based steering turn unless one is going on a straight line on flat terrain. These deterministic slips are easy to calculate for Ackerman steered motions on flat ground and are used as approximations to the true deterministic slip even during motion over non-flat terrain. Another deterministic slip

constraint measurement can be derived from experiments. For example, over sandy terrain, a known rate of experimentally derived longitudinal (x) slip during traverses can be added as a non-zero t_m term.

A slip action that is only modeled statistically is due to the wheel-ground interaction at each individual wheel. Consider the case when each wheel is driven by a control algorithm that attempts to maximize compliance of the wheel-ground rolling interaction, and also maximally coordinates the control effort across all the wheels. Then the slips at each wheel in the longitudinal (x) rolling direction are mostly independent of each other. Now consider a rover in which each wheel is independently driven by a high-gain, "stiff" control algorithm. Then each wheel rotates to follow the setpoint established by the controller and does not accommodate to any wheel-ground forces of interaction. The slips at each wheel are thus strongly correlated.

Another statistically modeled slip action is due to the terrain curvature. As the vehicle makes progress on the terrain, the rocker-bogey mechanism mostly accommodates the vehicle to maintain contact over the terrain and a highly compliant wheel controller can zero out any rolling slip. However, there is usually some inevitable transverse slip at each wheel to accommodate the curvature changes of the surface at each wheel contact. This slip can be modeled as a zero-mean process with time constants and dynamics related to the rate of change of surface curvature parameters along the rover path.

In actual practice, the slip at the wheel is a combination of all of the above processes. We choose not to model all the statistically describable noise terms in all of their complexity. Instead we select a simple uncorrelated slip model for our early implementations, with the covariance strengths determined by experiments. There may also be opportunities to develop a true slip related measurement using the motor current data on the drive motors.

3 Experiments

Test data is obtained from Rocky-7 operated in the JPL Mars Yard, a 15 X 25 meter outdoor test area that closely simulates Mars-like terrain. Another source is a high-fidelity kinematic simulator of the rover contact kinematics [20]. This simulator solves for the contact configuration for a set of closely spaced points along a specified rover path. It then uses the contact geometry and surface parameters of the wheel and ground to derive wheel motion. As such the results correspond to the case of highly compliant control at each wheel minimizing slip in the rolling direction.

In all cases the slip measurement/constraint knowledge made available to the estimator is taken to be nominally zero for the translational motions. In case of turning motions, a non-zero slip value is calculated for the bogey wheels based upon the nominal steering rate. Of course, the statistical models of the slip "noise" allow the estimator to optimally utilize (or discount) the value of the nominal slip knowledge.

We report results for two test setups, with an emphasis on showing the contact point state estimation.

3.1 Simulated Data Results

Figure 3 shows the rover at the start of a 1 meter straight-line motion over the undulating surface. We

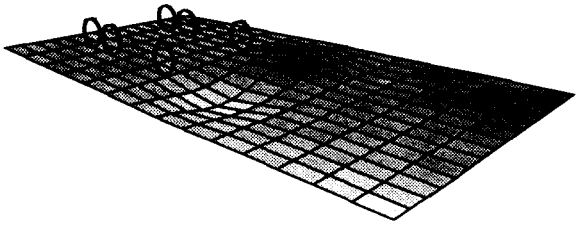

Figure 3: Simulated Motion On Undulating Terrain

can compare the performance of the kinematic estimator with one based upon dead-reckoning. The averaged wheel odometery obtained by integrating the speed (as indicated at each wheel) results in an estimate of distance traveled as 1.0204 m, i.e. approximately a 2% error over the actual distance traveled. For this straight-line motion one could correct this estimate by using the instantaneous vehicle pitch angle to project the wheel-derived traversal speeds prior to integration. However, this results in negligible improvement since the rocker-bogey mechanism keeps the pitch angles below 0.5 degrees for the entire duration of the motion. With the kinematic estimator we can correct for the effects of the nonlinear internal kinematics and the variations in contact angles at all of the wheels. The distance traveled is then estimated to be 1.0036 m indicating a much improved 0.3% error over the distance traveled.

We note that cross-track error reached a maximum of 14 mm. This is a result of a one-directional, terrain curvature induced transverse slip active for the portion

of the motion. Over a larger section of terrain this slip component would average out to zero resulting in only a small cross-track error on average.

The ground-truth contact points and the estimated values are shown in Figure 4. We observe that the tracking of the contact points is quite accurate, although with some lag.

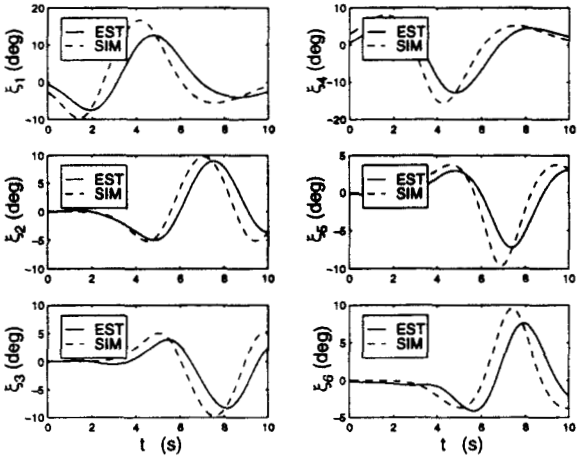

Figure 4: Ground-Truth and Estimate For Contact

3.2 Experimental Data Results

The control algorithm used on the rover consists of individual high-gain controllers on each wheel with no wheel coordination. The motion for this test set consists of a straight-line traverse on flat terrain with a single obstacle encountered by the right wheels (wheels 4,5,6). The obstacle is successfully traversed with the rover coming to rest with a portion of the right bogeys (wheels 5,6) resting on the obstacle. The obstacle causes two simultaneous effects. It results in a rover pitch-up as the wheels negotiate the obstacle as well as a change in the roll angle. Due to the momentum of the rover motion, there is minimal change in the rover heading.

The estimated attitude angles are shown in Figure 5 where we observe the roll and pitch deflections induced by the obstacle. The estimated positions and velocities are shown in Figure 6. We see that that the estimator has correctly picked up the z-deflection cause by the obstacle that results in an increase in vehicle height. Estimated contact states are shown in Figure 7. We note that the contact angle variations are quite large under the right wheels as would be expected by the traversal of those wheels over the obstacle. Since the final configuration of the rover is such that the

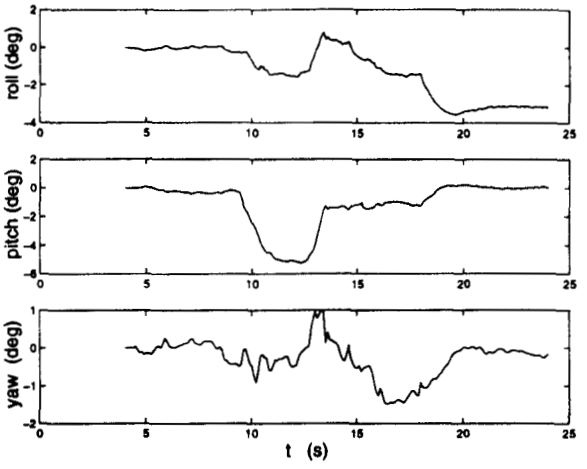

Figure 5: Estimate For Attitude

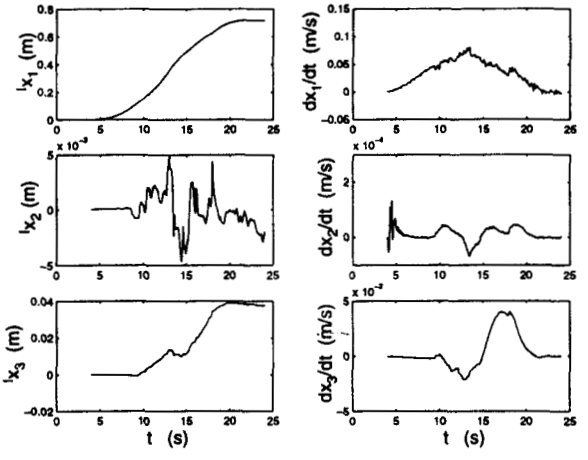

Figure 6: Estimate For Position and Velocities

right-side bogey wheels are in the middle of traversing the obstacle, the corresponding contact points are significantly displaced from zero at the end of the motion. However, the contact point for the right front wheel returns to near zero as it proceeds on level ground after climbing over the obstacle. As expected the wheels on the left side of the vehicle experience very little change in contact angles. The estimated position values are within 1 cm of the ground-truth data and the estimated contact angles are within 5 degrees.

4 Conclusions

By use of the slip-constraint concept, we have incorporated the non-linear kinematics, contact point geometry, and slip behavior into an Extended Kalman

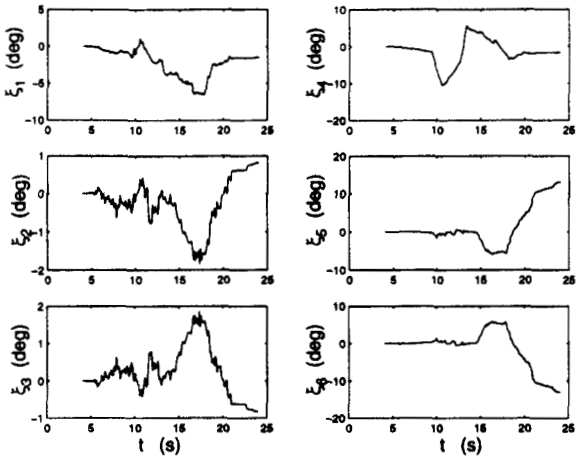

Figure 7: Estimate For Contact Angles

filtering framework. We have demonstrated improved odometery when this kinematic information is used in a complementary fashion with other on-board sensors. Future work items include:

- Sensor monitoring by means of filter residuals
- Mode switching between different estimator banks triggered by changes in observability.
- Incorporating a smoother to post-process the sensor data every time the rover obtains a precise attitude estimate during one of its periodic halts.
- Implementing sub-optimal filters with guaranteed response times.

Acknowledgments

This research was performed at the Jet Propulsion Laboratory, California Institute of Technology, under contract with the National Aeronautics and Space Administration.

Appendix A Filter Structure

We consider a simple rover model with just one translation degree-of-freedom with process model:

$$\begin{bmatrix} \dot{\theta} \\ \dot{x} \\ \dot{v} \\ \dot{b} \end{bmatrix} = \begin{bmatrix} \omega_m + b + n_1 \\ v \\ a_m + g\theta + n_2 \\ n_3 \end{bmatrix} \tag{11}$$

where θ is a single rotation angle, x is the translation, v is the velocity, b is the bias. The gyro measurement ω_m and the accelerometer measurement a_m enter into the process equation. Notice the gravity projection term $g\theta$ that is valid for small angles θ. The n_1, n_2, n_3 are the noise values. The measurement equation is given by:

$$\begin{bmatrix} \theta_m \\ x_m \\ v_m \end{bmatrix} = \begin{bmatrix} \theta + n_4 \\ x + n_5 \\ v + n_6 \end{bmatrix} \tag{12}$$

Here θ_m represents a measurement of the angle, x_m represents a measurement of the position, and v_m is a measurement of translational velocity. The n_4, n_5, n_6 are the noise values. Notice that velocity measurement is equivalent to a "slip" measurement in the form of $v - r\dot{\psi}$ where r would be a wheel radius and $\dot{\psi}$ would be the wheel rotational rate.

Consider an observer [10] for this system and the resulting closed loop transfer function of the observor. We only show one of these transfer functions, namely the term for estimate $\hat{\theta}(s)$. The other transfer functions show a similar complementary structure.

$$\hat{\theta}(s) = \theta_m(s)\frac{a(s)}{z(s)} + \omega_m(s)\frac{b(s)}{z(s)} + x_m(s)\frac{c(s)}{z(s)} + v_m(s)\frac{d(s)}{z(s)} + a_m(s)\frac{e(s)}{z(s)} \tag{13}$$

Here a, b, c, d, e, and z are polynomials in s with coefficients that are a function of the observor gains and g. The steady state Kalman filter would be obtained by selecting optimum values of the gains which then would be functions of the noise covariances. We can show that the following properties hold:

$$\frac{a(s)}{z(s)} + s\frac{b(s)}{z(s)} - g\frac{e(s)}{z(s)} = 1 \tag{14a}$$

$$c(s) + sd(s) + s^2e(s) = 0 \tag{14b}$$

Rearranging (13) we obtain:

$$\hat{\theta}(s) = \theta_m(s)\left[\frac{a(s)}{z(s)}\right] + \frac{\omega_m(s)}{s}\left[\frac{sb(s)}{z(s)}\right] + \frac{-a_m(s) + sv_m(s)}{g}\left[\frac{gd(s)}{sz(s)}\right] + \frac{-a_m(s) + s^2x_m(s)}{g}\left[\frac{gc(s)}{s^2z(s)}\right] \tag{15}$$

Each of the terms represents a weighted measurement of θ with the weights being the terms in the square brackets. The sum of all the weighting terms adds to 1 indicating the complementary nature of the filter.

References

[1] B. Barshan, and H.F. Durrant-Whyte, "Inertial navigation systems for mobile robots," *IEEE Trans. on Robot. and Automat.*, 11 (3), pp. 328-242, 1995.

[2] E.T. Baumgartner and S.B. Skaar, "An autonomous vision-based mobile robot," *IEEE Trans. on Automat. Control*, 39(3), pp. 493-502, 1994.

[3] J. Borenstein and L. Feng, "Gyrodometry: A new method for combining data from gyros and odometry in mobile robots," *Proc. 1996 IEEE ICRA*, pp. 423-428, Minneapolis, 1996.

[4] R.G. Brown, "Integrated Navigation Systems and Kalman Filtering", *Journal of The Institute of Navigation*, 19 (4), Winter 1972-73.

[5] J. Fraden, *AIP Handbook of Modern Sensors: Physics, Designs, and Applications*, American Institute of Physics, New York, 1993.

[6] Y. Fuke and E. Krotkov, "Dead Reckoning for a Lunar Rover on Uneven Terrain," *Proc. 1996 IEEE International Conference on Robot. and Automat.*, pp. 411-416, Minneapolis, Minnesota, April 1996.

[7] A. Gelb, ed., *Applied Optimal Estimation*, The M.I.T. Press, Cambridge, 1974.

[8] K.R. Kim, J.C. Lee and J.H. Kim, "Dead-reckoning for a Two-wheeled Mobile Robot on Curved Surfaces," *Proc. 1996 IEEE International Conference on Robot. and Automat.*, pp. 1732-1737, Minneapolis, Minnesota, April 1996.

[9] J.J. Leonard and H.F. Durrant-Whyte, "Mobile Robot Localization by Tracking Geometric Beacons," *IEEE Trans. on Robot. and Automat.*, 7 (3), pp. 376-382, 1991.

[10] D. G. Luenberger, "An Introduction to Observer," IEEE Trans. Automatic Control, AC-16 (6), 1971.

[11] R. Madhavan, M.W.M.G. Dissanayake, and H.F. Durrannt-Whyte, "Autonomous Underground Navigation of an LHD using a Combined ICP-EKF Approach," *Proc. 1998 IEEE Int. Conf. on Robot. and Automat.*, Leuven, pp. 3703-3708, Belgium, May 1998.

[12] L. Matthies, *Dynamic Stereo Vision*, Ph.d. Thesis. Computer Science Department, Carnegie Mellon University, 1987.

[13] D.J. Montana, "The Kinematics of Contact and Grasp," *The Int. J. Robotics Research*, 7 (3), pp. 17-32, 1988.

[14] R.M. Murray, Z. Li and S.S. Sastry, *A Mathematical Introduction to Robotic Manipulation*, CRC Press, Boca Raton, Florida, 1994.

[15] C. Olson, "Mobile Robot Self-Localization by Iconic Matching of Range Maps," *Proc. of the 8th International Conference on Advanced Robotics*, pp. 447-452, 1997.

[16] S. Roumeliotis and G. Bekey, "An Extended Kalman Filter for frequent local and infrequent global sensor data fusion," *Proc. SPIE - Sensor Fusion and Decentralized Control in Auton. Robotic Systems*, 3209, pp 11-22, Pittsburgh, 1997.

[17] R. E. Scheid, D. S. Bayard, J. Balaram and D. B. Gennery, "On-board State Estimation for Planetary Aerobots," *AIAA Intl. Balloon Technology Conf, AIAA 97-1462*, June 3-5, 1997, San Fransisco, USA.

[18] J. Vaganay and M.J. Aldon, "Attitude Estimation For A Vehicle Using Inertial Sensors," *Control Eng. Practice*, 2 (2), pp. 281-287, 1994, Elsevier.

[19] R. Volpe, J. Balaram, T. Ohm and R. Ivlev. "Rocky 7: A Next Generation Mars Rover Prototype." Journal of Advanced Robotics., 11(4), December 1997.

[20] J. Yen, A. Jain and J. Balaram, "ROAMS : Rover Analysis, Modeling and Simulation Software," *Fifth International Symposium on Artificial Intelligence and Automation in Space*, Noordwijk, The Netherlands, 1-3 June 1999.